

Spin excitations of half-doped bilayer manganites: intermediate phase

Ivon R. Buitrago^{1,2}, Cecilia I. Ventura^{2,3}, and Luis O. Manuel⁴

¹ Instituto Balseiro, Univ. Nac. de Cuyo and CNEA, 8400-Bariloche, Argentina

² (CONICET) Centro Atómico Bariloche-CNEA, Av. Bustillo 9500, 8400-Bariloche, Argentina

³ Universidad Nacional de Río Negro, 8400-Bariloche, Argentina

⁴ Instituto de Física Rosario (CONICET-UNR), Rosario, Argentina.

E-mail: ivonnebuitrago@cab.cnea.gov.ar

Abstract. Few magnon measurements in half-doped manganites are available. Recently, the spin-wave spectrum of half-doped bilayer $\text{Pr}(\text{Ca}_{0.9}\text{Sr}_{0.1})_2\text{Mn}_2\text{O}_7$ was reported (*Johnstone et al 2012 Phys.Rev.Lett.***109** 237202). The best fit included, using a localized spin model, corresponds to a ground state with a combined spin, charge and orbital ordering analogous to the CE phase proposed by Goodenough in 1955, though with a quite larger Mn-charge disproportionation. The latter contradicts previous experimental indications in half-doped manganites, pointing toward smaller Mn-disproportionations: in a range between the minimum value corresponding to the Zener-polaron or dimer phase (with all Mn-charges formally equal to 3.5+), and the maximum disproportionation found in Goodenough's CE phase (with Mn^{3+} and Mn^{4+}). Such indications led to the intermediate phase proposal (*Efremov et al 2004 Nat.Mats.***3** 853). Here, we analyze the spin excitations of half-doped bilayer (and layered) manganites, calculating them in terms of a localized spin model suitable to describe the intermediate, CE and dimer phases. We discuss the effects of an extensive set of magnetic couplings, including all those introduced in previous fits. An improved description of the magnons reported for bilayer manganites is obtained assuming a generalized CE phase with Mn-disproportionation inside the expected range, by including next-nearest-neighbour magnetic coupling parameters between the planar Mn zig-zag chains.

PACS numbers: 75.10.-b,75.25.Dk,75.30.Ds,75.47.Gk

Keywords: Magnetic excitations, intermediate phase, manganites

1. Introduction

The doped manganite oxides have the general formula $(A_{1-x}B_xMnO_3)_nBO$, where A and B respectively are trivalent rare-earth-metal and divalent alkaline-earth-metal ions, and n is the number of perovskite blocks separated by rock salt-structure non-magnetic BO layers. Thus, $n = 1$ represents the layered structure $A_{1-x}B_{1+x}MnO_4$, $n = 2$ the bilayer $A_{2-2x}B_{1+2x}Mn_2O_7$, and $n \rightarrow \infty$ the three-dimensional $A_{1-x}B_xMnO_3$. Due to the strong correlations between charge, orbital and spin degrees of freedom, these manganese oxides exhibit rich phase diagrams, including ferromagnetic metallic phases (FM-M), antiferromagnetic insulating phases (AF-I) with charge and orbital order (CO-OO), among others which are of technological interest [1, 2, 3, 4]. At low doping ($x \sim 0.3$), some of these compounds exhibit the interesting phenomenon of colossal magnetoresistance (CMR), which has been found in three dimensional manganites $A_{1-x}(Sr,Ca)_xMnO_3$ [5] and bilayer manganites such as $La_{2-2x}Sr_{1+2x}Mn_2O_7$, and only above high magnetic fields in layered $La_{1-x}Sr_{1+x}MnO_4$ [6, 7].

For three-dimensional perovskite manganites, in 1955 Goodenough [8] predicted the magnetic, charge and orbital ordering for $La_{1-x}B_xMnO_3$ valid in the whole doping range: $0 \leq x \leq 1$, based on his hypothesis of covalent/semicovalent bonds and the Zener double-exchange [9] picture. In particular, at half-doping ($x = 0.5$) he proposed the antiferromagnetic CE phase. This phase is characterized by an arrangement of charges and spins, such that in the MnO_2 planes the $Mn^{(3.5-\delta)+}$ and $Mn^{(3.5+\delta)+}$ ions, where $\delta = 0.5$ is a measure of the Mn-charge disproportionation (CD), form a checkerboard pattern and equal charges are stacked one above the other in the direction perpendicular to the planes. The spins of Mn^{3+} (S_1) and Mn^{4+} (S_2) ions form ferromagnetic zig-zag chains which are antiferromagnetically coupled among them, in the planes and between them. The corner sites in the zig-zag chains are occupied by Mn^{4+} , whereas the bridge sites are occupied by Mn^{3+} . This charge order seemed to agree with several experimental results. Based on synchrotron X-ray diffraction (SXRD) and neutron powder diffraction (ND) data on $La_{0.5}Ca_{0.5}MnO_3$, Radaelli *et al.* [10] proposed a superstructure with three inequivalent Mn sites which could explain their results: two Mn^{3+} sites (differing only in the degree of distortion of the MnO_6 octahedra they form) and a Mn^{4+} one, being the charge order coupled to magnetic and orbital orders. Also by SXRD, in $La_{0.5}Sr_{1.5}MnO_4$ Murakami *et al.* [11] indicated that they could directly observe the Mn^{3+}/Mn^{4+} pattern, as well as a simultaneous orbital ordering of the e_g electrons of Mn^{3+} . However, they were unable to determine univocally the orbital ordering, because they obtained the same results assuming a $3x^2 - r^2/3y^2 - r^2$ pattern or a $y^2 - z^2/3z^2 - x^2$ one. Using X-ray scattering at the Mn K-edge on $LaSr_2Mn_2O_7$ and *ab-initio* calculations, Di Matteo *et al.* [12], concluded the same by showing that the intensity of the forbidden Bragg reflections measured could be attributed to the Jahn-Teller distortions (JTD) of oxygen octahedra, rather than to an orbital ordering of e_g electrons on the Mn^{3+} sites.

Although these and other studies showed evidence of charge order in agreement with Goodenough's model [8], with the refinement of the crystal structure of $Pr_{0.6}Ca_{0.4}MnO_3$ obtained by neutron diffraction by Daoud-Aladine *et al.* [13], in which no evidence of charge ordering was found, the proposal of Goodenough's CE ground state for these compounds was questioned. To explain their measurements, Daoud-Aladine *et al.* [13] proposed the Zener polarons dimer phase (ZP), in which instead of Mn^{3+} and Mn^{4+} charge ordering as in the CE structure, there is an electron delocalized

between each pair of Mn ions, due to the double-exchange mechanism, and the Mn ions are considered to form spin dimers, having an intermediate valence $\text{Mn}^{3.5+}$ ($\delta = 0$). From X-ray diffraction data on the same manganite, Grenier *et al.* [14] argued that there are two inequivalent Mn sites accompanied by an orbital order, but they did not obtain evidence of a CD between the two Mn ions, in agreement with Daoud-Aladine *et al.* [13]. Furthermore, with soft X-ray diffraction in the same compound, Hill *et al.* [15] suggested that the Mn sites were highly mixed between the Mn^{3+} and Mn^{4+} formal oxidation states with two inequivalent Mn sites, since the shift in the shape and the change in the spectral line weights corresponding to magnetic and orbital diffractions did not match the ionic model of Goodenough's CE phase. Last year, from their ESR study and magnetic susceptibility $\chi(T)$ measured in $\text{Y}_{0.5}\text{Ca}_{0.5}\text{MnO}_3$, Winkler *et al.* [16] interpreted the change of regime they found in $\chi(T)$ between 100 and 200 K, as due to charge dimerization in accordance with the proposal by Daoud-Aladine *et al.* [13]. They showed that the effective moment μ_{eff} and Curie constant, estimated assuming the formation of dimers like in the ZP phase, are quite consistent with those obtained from experiments. Other experimental studies in half-doped manganites support the idea of a charge disproportionation lower than in Goodenoughs CE phase (i.e. $\delta \leq 0.5$), but not zero either, as for the Zener polaron model. Indeed, with their results of X-ray resonance (RXS) at the Mn K edge of $\text{Nd}_{0.5}\text{Sr}_{0.5}\text{MnO}_3$, Herrero *et al.* [17], indicated that charge order was not necessary to explain the data, since two Mn sites with different local geometries existed: one with distorted oxygen octahedra and one without distortion, in accordance with Di Matteo *et al.* [12]. In particular, they found charge states $\text{Mn}^{3.42+}$ and $\text{Mn}^{3.58+}$, corresponding to $\delta = 0.08$. The same was reported for $\text{Bi}_{0.5}\text{Sr}_{0.5}\text{MnO}_3$, where Subias *et al.* [18], with the same method of Ref.[17], found a charge imbalance of $\Delta n = 0.14e^-$ between two Mn sites (though it was not possible to define the valence states of each Mn ion), while for layered $\text{La}_{0.5}\text{Sr}_{1.5}\text{MnO}_4$ Herrero *et al.* [19] obtained $\Delta n = 0.15e^-$, using also SXPD.

Given the growing debate on the two main scenarios proposed for the ground state of half-doped manganites, in 2003 Ventura and Alascio [20] studied the spin dynamics which would result from a charge ordered (CO) phase and the ZP dimer phase, calculating the respective magnons using a model of localized spins. Differences between the magnon dispersion of these phases were found, which should make it possible to distinguish them through inelastic neutron scattering (INS) experiments [20]. Indeed, now INS data exist in half-doped manganites, by which it was attempted to shed light on the nature of the ground state and the charge disproportionation present. For the layered manganite $\text{La}_{0.5}\text{Sr}_{1.5}\text{MnO}_4$, the lower magnon bands measured by INS (below the magnon gap) by Senff *et al.* [21], could be fitted using a localized spin model in terms of a generalized CE phase, with spins $S_1 = 2$ and $S_2 = 1.5$ corresponding to Mn^{3+} and Mn^{4+} ($\delta = 0.5$, and $\Delta n = 1e^-$), with the inclusion of next-nearest-neighbor (NNN) intra-chain couplings between Mn^{4+} ions [21]. For the three-dimensional perovskite manganite $\text{Nd}_{0.5}\text{Sr}_{0.5}\text{MnO}_3$, Ulbrich *et al.* [22] found necessary, besides the coupling terms introduced in Ref. [21], to consider $S_1 = 1.79$ and $S_2 = 1.67$ spins, corresponding to $\text{Mn}^{3.42+}$ and $\text{Mn}^{3.66+}$ ($\Delta n = 0.24e^-$). Notice that in Refs.[21, 22]) only magnon bands below ~ 40 meV were reported. More recently, in the work of Johnstone *et al.* [23] on the bilayer compound $\text{Pr}(\text{Ca}_{0.9}\text{Sr}_{0.1})_2\text{Mn}_2\text{O}_7$ two alternative generalized CE ground states were presented as the most satisfactory fits they found to their INS data. One, includes exchange couplings up to NNN within the zig-zag chains, between spins on the corner sites (as in Refs.[21, 22]) and among the bridge sites, being corner and bridge sites occupied by

equal spins [23] of magnitude $S_1 = S_2 = 7/4$. The alternative fit corresponds to a CE phase, without NNN couplings, but with spins of respective magnitudes $S_1 = 2.16$ and $S_2 = 1.34$, corresponding to $\text{Mn}^{2.68+}$ and $\text{Mn}^{4.32+}$ (i.e. $\Delta n = 1.68e^-$): thus, assuming a charge disproportionation $\delta = 0.82$ which is outside the range $0 \leq \delta \leq 0.5$ indicated by most experiments.

In this context, and discussing the possibility of multiferroicity in some manganese compounds and other magnetic systems [24, 25], Efremov, Van den Brink and Khomskii [26] proposed a new phase that could be relevant: the *intermediate* phase (IP). This phase consists of spin dimers (thus incorporating aspects of the Zener polaron phase proposed by Daoud-Aladine et al.[13]), though formed by a pair of parallel Mn spins of different magnitude, in principle (thereby allowing for a degree of Mn charge disproportionation: not necessarily as large as that of Mn^{3+} - Mn^{4+} in Goodenough's original CE phase[8]). In the intermediate phase, consecutive spin dimers located along the planar zig-zag chains are oriented at a constant relative angle between them. Varying the charge disproportionation and angle between the dimers, the intermediate phase could allow to continuously interpolate between the two limiting cases represented by: the CE phase and the dimer phase denoted as "orthogonal intermediate $\pi/2$ -phase". In 2009 Giovannetti *et al.* [27], through a theoretical study in a microscopic degenerate double-exchange (DDEX) model, with density functional theory (DFT) calculations indicated that an intermediate state as proposed by Efremov et al. [26] would explain the possible ferroelectricity of $\text{La}_{0.5}\text{Ca}_{0.5}\text{MnO}_3$, and in turn they found a maximum $\Delta n = 0.2e$ between Mn ions (i.e. $\text{Mn}^{3.4+}$ - $\text{Mn}^{3.6+}$) when the intersite Coulomb interaction $U \rightarrow \infty$. In another work, Barone *et al.* [28], include the effect of bulking of the oxygens through the hopping between Mn-Mn in zig-zag chains in the DDEX model studied by Giovannetti *et al.* [27], and show that this would favor the dimerization of the Mn ions, and therefore lead to lower charge disproportionation than expected in Goodenough's CE phase [8]. Recently, Yamauchi and Picozzi [29] used DFT calculations to estimate the Born Effective Charge (BEC) tensor for three-dimensional $\text{Pr}_{0.5}\text{Ca}_{0.5}\text{MnO}_3$ and bilayer $\text{Pr}(\text{Ca}_2)_2\text{Mn}_2\text{O}_7$, assuming CE and ZP phases. In the case of the three-dimensional manganite it was found that in the CE phase there would exist $\Delta n = 0.5e^-$ between Mn^{3+} and Mn^{4+} ions, while in the ZP phase, where ideally $\Delta n = 0$, a small but not zero charge disproportionation Δn between the corner and bridge Mn ions is obtained, consistent with the proposal by Efremov *et al.* [26].

In this work, we explore the ground state of half-doped manganites indirectly, by calculating the magnetic excitations for the bilayer intermediate phase. In the following sections, we present the model proposed for the intermediate phase of bilayer manganites, as an extension of that already proposed in Ref. [30] for the layered case, within a localized spins scheme, where we include couplings already considered in Refs. [21, 22, 23], and AF (NNN) couplings for inter-chain sites in planes. With the same method as in Ref. [30] we exhibit the main effects of the different couplings on the different bands. Finally we discuss the results obtained by Senff et al. [21] in layered manganite $\text{La}_{0.5}\text{Sr}_{1.5}\text{MnO}_4$ and by Johnstone et al. [23] in bilayer manganite $\text{Pr}(\text{Ca}_{0.9}\text{Sr}_{0.1})_2\text{Mn}_2\text{O}_7$, and for the bilayer compounds present two alternative fits to those proposed by Johnstone [23], which have the advantage of not requiring NNN intra-chain couplings and in addition keep the charge disproportionation within the expected range suggested by most experiments.

2. Model for the intermediate phase, and magnon calculation method

To describe the intermediate phase [26] of half-doped bilayer manganites, we consider a model of localized spins. As for the layered compounds in our previous work [30], the intermediate phase introduced by Efremov, van den Brink and Khomskii in 2004 [26] is represented by spin dimers (thus incorporating aspects of the Zener polaron phase (ZP) proposed in 2002 by Daoud-Aladine et al. [13]), formed by a pair of parallel Mn spins which could be of different magnitude, in principle, thereby allowing for a degree of Mn charge disproportionation. We denote the respective spin magnitudes in a dimer by S_1 and S_2 , corresponding to $\text{Mn}^{(3.5-\delta)+}$ and $\text{Mn}^{(3.5+\delta)+}$ ions: δ being a measure of the Mn-charge disproportionation (CD). In the intermediate phase, consecutive spin dimers located along the planar zig-zag chains are oriented at a constant relative angle θ between them, as shown in figure 1. Notice that the zig-zag chains are antiferromagnetically coupled between them in the planes, as well as in the (z) direction perpendicular to the planes, while along z equal charges (spin magnitudes) are stacked one on top of another.

Varying the Mn-charge disproportionation δ and the angle θ , this intermediate phase would allow to continuously interpolate between Goodenough's CE phase ($\delta = 0.5$, $\theta = 0$), and the dimer phase denoted as the "orthogonal intermediate $\pi/2$ -phase" ($\delta = 0$, $\theta = \pi/2$). Notice that in the latter $\pi/2$ -phase [26] consecutive dimers would have their spins oriented perpendicularly, in contrast to Daoud-Aladine's ZP phase [13] where all dimers in a zig-zag chain have parallel spins: these two dimer phases as well as a generalized CE phase were analyzed as possible electronic ground states for the fits to the magnons recently measured [23].

Here, in order to analyze their effects and identify those most relevant to improve the description of the experimental INS results so far available in half-doped manganites, we have considered a wide range of magnetic couplings, including all those previously introduced in the fits to experiments by other groups as well as a few additional ones, as shown in figure 1.

Concretely, the magnetic couplings analyzed were: along the zig-zag chains, two intra-chain nearest-neighbor (NN) ferromagnetic couplings: intra-dimer F' and inter-dimer F ; an inter-chain NN antiferromagnetic coupling A ; an intra-chain next-nearest-neighbor (NNN) ferromagnetic coupling F_c between (S_2 - S_2) corner spins; a single-ion anisotropy D (the previous couplings were considered in the experimental fits of Refs. [21, 22, 23]); along z : two inter-plane antiferromagnetic couplings, allowing for eventual spin differentiation, i.e. A_z between S_1 - S_1 spins and B_z among S_2 - S_2 spins (as used in our previous work [31], while $A_z = B_z$ was assumed in Refs. [22, 23]); and, as in our previous study of the layered half-doped manganites [30]: an intra-chain NNN antiferromagnetic A_d between S_1 - S_1 coupling (also discussed in Ref. [23]), and an inter-dimer biquadratic (BQ) coupling term K along the zig-zag chains.

Furthermore, for the intermediate phase at non-zero θ angles, taking into account that the rotation (canting) between inter-chain spins might weaken some antiferromagnetic couplings: the possibility of a differentiation of the AF (NN) inter-chain coupling was analyzed, hence we have couplings A between non-rotated dimer-spins, and A' between spins in rotated dimers (as depicted in figure 1). Finally, we studied the effect of NNN coupling terms between the zig-zag chains: these proved relevant to improve the fit of the magnetic excitations in $\text{Pr}(\text{Ca}_{0.9}\text{Sr}_{0.1})_2\text{Mn}_2\text{O}_7$, reproducing a dispersion missing in previous fits by other groups, as will be discussed in section 4. To be able to take into account spin differentiation (charge

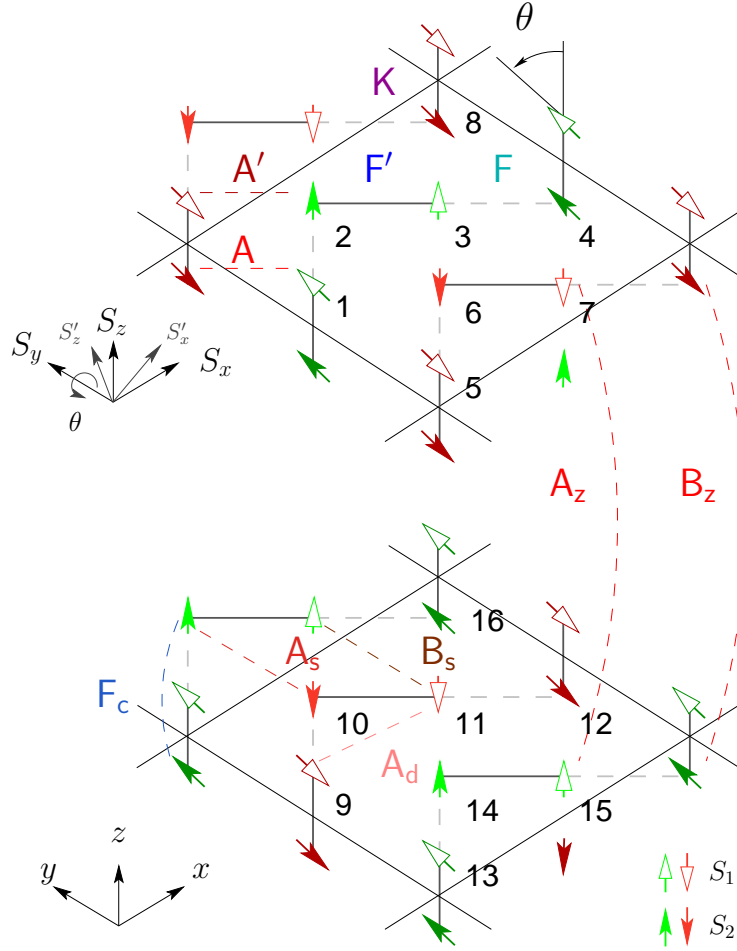


Figure 1. (Color online) Schematic representation of the unit cell for the intermediate phase studied, representing by empty and filled arrows the $\text{Mn}^{(3.5-\delta)+}$ (S_1) and $\text{Mn}^{(3.5+\delta)+}$ (S_2) sites, respectively. Along the zig-zag chains, spin dimers can be identified by the solid lines representing the intra-dimer ferromagnetic coupling F' , which alternate with dashed lines representing the inter-dimer ferromagnetic coupling F . The rotation of the spin quantization axes, around S_y , between the spins of consecutive dimers on a zig-zag chain is described by angle θ . All magnetic couplings shown, are described in the text.

disproportionation) effects, we studied the following inter-chain NNN couplings: A_s between S_2 - S_2 spins, and B_s between S_1 - S_1 spins.

In table 1 we summarize the parameters characteristic of some specific phases proposed for half-doped manganites, in terms of the parameters of this model.

Table 1. Model parameters characterizing specific magnetic phases.

Goodenough's CE phase $\theta = 0$	Orthogonal $\pi/2$ phase $\theta = \pi/2$	ZP dimer phase $\theta = 0$
$S_1=2$	$S_1 = 1.75$	$S_1 = 1.75$
$S_2=1.5$	$S_2 = 1.75$	$S_2 = 1.75$
$F = F'$	$F < F'$	$F < F'$
$A' = A$	$A' < A$	$A' = A$

For a concrete implementation of the intermediate phase, able to interpolate between Goodenough's CE phase ($\delta = 0.5$, $\theta = 0$), and the "orthogonal intermediate $\pi/2$ -dimer phase" ($\delta = 0$, $\theta = \pi/2$), we have considered the same angular dependence for F , S_1 and S_2 previously used for the layered compounds [30], now also including angular dependence in coupling A' , so that:

$$F = F' \cos\left(\frac{2\theta}{3}\right), \quad A' = A \cos\theta, \quad (1a)$$

$$S_1 = \frac{7}{4} + \frac{1}{4} \cos\theta, \quad S_2 = \frac{7}{4} - \frac{1}{4} \cos\theta. \quad (1b)$$

Notice, that in this case: $\delta = 0.5 \cos\theta$.

With these magnetic couplings the Hamiltonian is given by:

$$\begin{aligned}
H = & -F' \sum_{\langle i,j \rangle \in C,D} \mathbf{S}_i \cdot \mathbf{S}_j - F \sum_{\langle i,j \rangle \in C \notin D} \mathbf{S}_i \cdot \mathbf{S}'_j + A \sum_{\langle i,j \rangle \notin C} \mathbf{S}_i \cdot \mathbf{S}_j \\
& + A' \sum_{\langle i,j \rangle \notin C} \mathbf{S}_i \cdot \mathbf{S}'_j + K \sum_{\langle i,j \rangle \in C, \notin D} (\mathbf{S}_i \cdot \mathbf{S}'_j)^2 - D \sum_i S_{iz}^2 \\
& + A_z \sum_{\langle i,j \rangle \notin P} \mathbf{S}_i \cdot \mathbf{S}_j + B_z \sum_{\langle i,j \rangle \notin P} \mathbf{S}_i \cdot \mathbf{S}_j + A_d \sum_{\langle\langle i,j \rangle\rangle \in C} \mathbf{S}_i \cdot \mathbf{S}'_j \\
& - F_c \sum_{\langle\langle i,j \rangle\rangle \in C} \mathbf{S}_i \cdot \mathbf{S}'_j + A_s \sum_{\langle\langle i,j \rangle\rangle \in C} \mathbf{S}_i \cdot \mathbf{S}_j + B_s \sum_{\langle\langle i,j \rangle\rangle \in C} \mathbf{S}_i \cdot \mathbf{S}_j
\end{aligned} \quad (2)$$

where C denotes spins in one zig-zag chain, D in a dimer, and P in a plane, the sums over $\langle i, j \rangle$ denote NN, while $\langle\langle i, j \rangle\rangle$ refer to NNN, as usual. \mathbf{S}'_j is used for rotated spins.

Using the above Hamiltonian, the classical energy per unit cell of the system is written as:

$$\begin{aligned}
E = & 8 \left[(A - F') S_1 S_2 + A_s S_2^2 + B_s S_1^2 \right] + 4 \left[(A_z - D) S_1^2 + (B_z - D) S_2^2 \right] \\
& + 8 \left[(A' - F) S_1 S_2 + A_d S_1^2 + (A_s - F_c) S_2^2 \right] \cos\theta \\
& + \left[8 K S_1^2 S_2^2 - 4 D (S_1^2 + S_2^2) \right] \cos^2\theta
\end{aligned} \quad (3)$$

Equation (3) will allow us to evaluate the classical energy per unit cell, in order to identify the parameters which are relevant to obtain a stable classical intermediate phase, as well as discuss some classical and quantum results in next section.

To determine the quantum magnetic excitations of the intermediate phase for bilayer half-doped manganites, we considered the 16-spin magnetic unit cell shown in figure 1. We first performed a local rotation of the spin quantization axes at an angle θ , for sites within the rotated dimers in Hamiltonian (2). The spins in the rotated system \mathbf{S}'_j are related to the fixed system ones \mathbf{S}_j as follows: $S_j^{y'} = S_j^y$,

$$S_j^x = S_j^{x'} \cos \theta - S_j^{z'} \sin \theta, \quad (4a)$$

$$S_j^z = S_j^{x'} \sin \theta + S_j^{z'} \cos \theta. \quad (4b)$$

Afterwards, we use the Holstein-Primakoff transformation for spin operators, Fourier transform, and determine the magnon excitations by paraunitary diagonalization [32] of the Hamiltonian matrix in the linear spin waves approximation, as in [30].

3. Results

Below, we present the most relevant results obtained in our classical and quantum investigation of the intermediate phase. We show, in particular, the effects of the different magnetic coupling parameters included in our model, allowing us to identify which parameters are most relevant to stabilize the magnetic excitations of the intermediate phase as a means of indirectly analyzing the stability of that proposed ground state, and which parameters enable us to exhibit an improved fit of the inelastic neutron scattering data for bilayer compounds recently reported in the literature [23]. In the following, all energy parameters mentioned will be expressed in meV, unless explicitly stated otherwise.

3.1. Effect of intra-chain inter-dimer biquadratic coupling K

As mentioned in previous section, in our model we included biquadratic coupling K , which was originally used by Cieplak [33] to study magnetic spins in mixed-valence three-dimensional manganites. Also, in a series of recent studies [34, 35, 36] of the spin dynamics exhibited by ferropnictide superconductors, biquadratic exchange terms were invoked as necessary ingredients to be added to an anisotropic Heisenberg Hamiltonian in order to describe the experimental results. [37, 38] We have studied the effect of K previously, in the context of our investigation of the magnons of layered half-doped manganites and the intermediate phase [30].

As shown in figure 2, this magnetic coupling allows to obtain classically stable intermediate phases with θ angles between 0 and $\pi/2$. K is the most relevant coupling for the stabilization of the classical intermediate phase without requiring the introduction of other NNN couplings, since it favors perpendicular arrangement of inter-dimer adjacent spins. Although in our model, to simplify the quantum magnon calculation, we introduced K only between dimers within a zig-zag chain, we checked that one could extend it to inter-chain neighbor sites without substantially altering its effect on the stabilization of the classical intermediate phase.

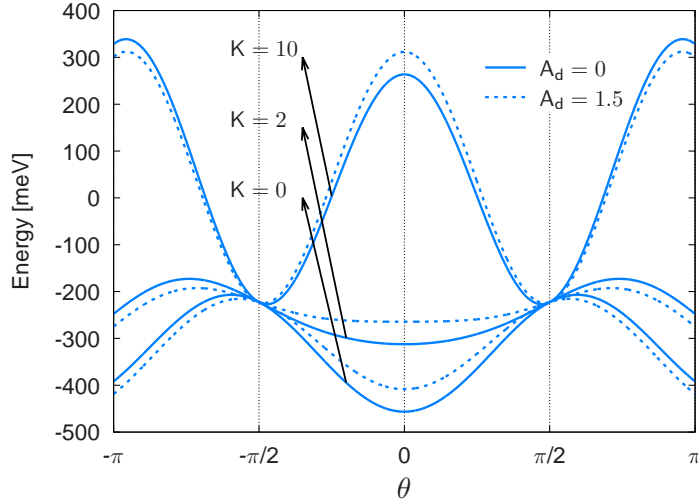


Figure 2. (color online) Bilayer: Angular dependence of the energy of the classical intermediate phase. Non-zero magnetic couplings, in meV: $F' = 11.39$, $A = 1.5$, $D = 0.074$, $A_z (= B_z) = 0.88$ (as in Ref.[23]). F as in equations (1a) and S_1, S_2 as in equations (1b). $A_d = 0$ (solid lines), $A_d = 1.5$ (dashed lines). The K dependence is indicated by arrows (for each solid line, and its adjacent dashed line).

With respect to the layered case [30], the main difference lies in the energy scales involved. Having only half of the K couplings, and $A_z (= B_z) = 0$, the range of values for the classical energy of the intermediate phase of layered compounds extends between -250 and 180 meV, in contrast to the range of -500 to 360 meV shown for bilayer compounds in figure 2. We have verified that the angle θ_{\min} (by which we denote the angle characteristic of the classical intermediate phase with minimal energy, which in general depends on K : as e.g. figure 2 shows), for each particular value of K is the same regardless of whether the system is layered or bilayered.

3.2. Differentiation of inter-chain couplings A y $A'(\theta)$

As seen in figure 3, including a differentiation in the antiferromagnetic coupling between chains, as described in section 2, allows to reduce the critical value of biquadratic coupling K_c above which a classical intermediate phase with $\theta \neq 0$ is stable, feature which we find is common to the layered and bilayer cases. Let us mention that for bilayer systems, $K_c = 0$ is attained for $A = 8.1$ meV and $A_z/A > 0.41$: case in which the ratio between A and F' is large compared to the values previously reported [21, 22] and therefore not relevant to fit the experimental data.

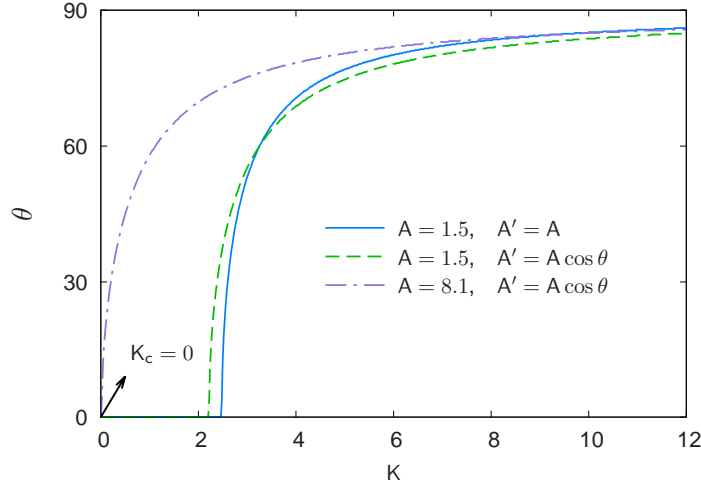


Figure 3. (color online) Bilayer: Angle characteristic of the classical intermediate phase with minimal energy, as a function of K : for various A and A' inter-chain couplings, as detailed in inset. Non-zero magnetic couplings, in meV: $F' = 11.39$, $A_z (= B_z) = 0.88$, $D = 0.074$. F as in equations (1a) and S_1, S_2 as in equations (1b). For: $A = A' = 1.5$ (solid line); $A = 1.5$, $A' = 1.5 \cos \theta$ (dashed line); $A = 8.1$, $A' = 8.1 \cos \theta$ (dash-dotted line).

Considering now the magnons of the quantum intermediate phase presented in figure 4, for couplings $A = 1.5$ meV and $A' = A \cos \theta$ corresponding to the classical case represented by the dashed-line of figure 3, it is evident that the effect of K is to widen the range of θ angles which lead to a stable quantum intermediate phase. In particular, the maximum angle θ_{max} below which a stable quantum intermediate phase exists is seen to shift from 8.83 degrees at $K = 0$, to 10.39 degrees at $K = 1.7$. Unless otherwise stated, all quantum magnon results appear plotted along symmetry paths in the square or cubic lattice Brillouin zones, depending on the case. Notice also that for the bilayer compounds we are using the same notation for the BZ of Ref.[23], since to take into account twinning effects it is necessary to double the unit cell in real space, so the points in reciprocal space here labelled as I and II, are given respectively by: I by X (or Y), and II by $(2\pi/a_x, \pi/a_y, 0)$ (or $(\pi/a_x, 2\pi/a_y, 0)$), where a_i denotes the lattice parameter along direction i ($i = x, y$). Comparing figure 3 and figure 4 it is clear that in both cases, $K = 0$ or $K = 1.7$, the quantum fluctuations lead to stable quantum intermediate phases with $\theta \neq 0$ in contrast with the corresponding stable classical phase, having $\theta = 0$. But it is worth mentioning that, using the same in-plane coupling parameters, we find that essentially the same θ_{max} value is obtained for the layered and the bilayer cases, in agreement with the classical result mentioned in previous subsection.

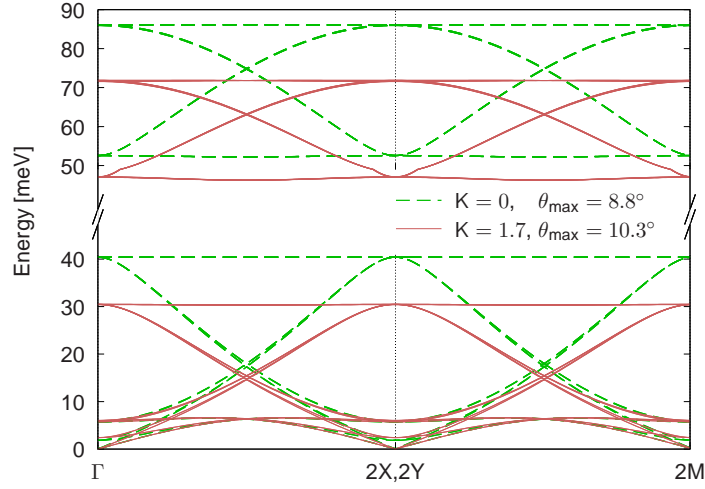


Figure 4. (color online) Bilayer: intermediate phase quantum magnons, for different K . Non-zero magnetic couplings, in meV: $F' = 11.39$, $A = 1.5$, $D = 0.074$; F and A' as in equations (1a), S_1 , S_2 as in equations (1b). For: $K = 0$ and $\theta = \theta_{\max} = 8.83$ degrees (dashed lines); $K = 1.7$ and $\theta = \theta_{\max} = 10.39$ degrees (solid lines).

3.3. Inclusion of intra-chain NNN couplings F_c and A_d

3.3.1. Layered compounds.

For $\text{La}_{0.5}\text{Sr}_{1.5}\text{MnO}_4$, Senff *et al.* [21] discussed the inclusion of NNN ferromagnetic couplings along the zig-zag chains: i.e. F_c and A_d in our notation of figure 1 and equation (2). They mention that both ferromagnetic couplings improve the fit of the magnetic excitations measured, favouring the addition of a non-zero F_c coupling to the basic parameters describing the CE phase. Our figure 5 shows that the effect of adding one or the other of these two couplings (with signs corresponding to ferromagnetic exchanges, for both) on the classical energy (and the resulting stable intermediate phase) is quantitatively different. For example, different values of K_c result if non-zero A_d or F_c of the same magnitude are included. This is due to the fact that the contribution to the classical energy by terms proportional to A_d is weighed by S_1^2 , whereas the contributions proportional to F_c appear weighed with S_2^2 , where $S_1 \geq S_2$ if charge disproportionation is present. In fact, in figure 5. we show how the magnon curves (line labelled by triangles, and dashed line) collapse together if these coupling parameters were accordingly rescaled: $A_d = -F_c S_2^2 / S_1^2$.

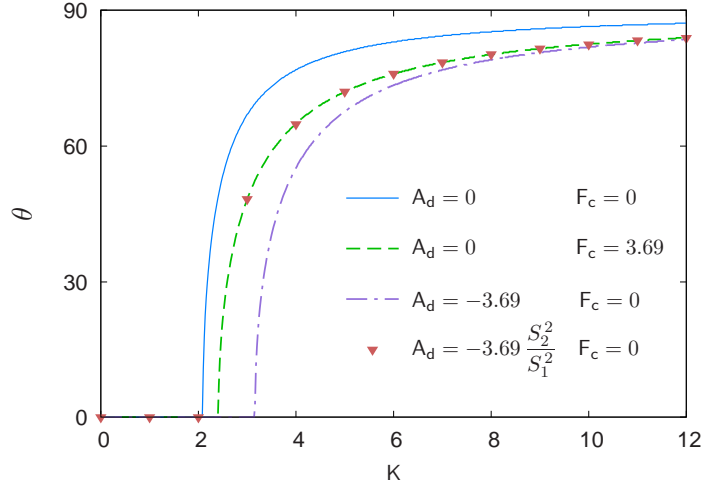


Figure 5. (color online) Layered: Angle characteristic of the classically stable intermediate phase, for different A_d and F_c combinations. Other non-zero magnetic couplings, in meV: $F' = 9.98$, $A = 1.83$, $D = 0.05$ (as in Ref.[21]); F and A' as in equations (1a), S_1 , S_2 as in equations (1b). For: $F_c = 0$, $A_d = 0$ (solid line); $F_c = 3.69$, $A_d = 0$, as in Ref [21] (dashed line); $F_c = 0$, $A_d = -3.69$ (dash-dotted line); $F_c = 0$, $A_d = -3.69 S_2^2/S_1^2$ (triangles).

In the quantum case, the effects of A_d and F_c differ even more: along the Brillouin zone, differences in the magnons are present even for cases where the classical curves collapse together, as we show in figure 6. While A_d increases the energies of the excitations in all paths of the Brillouin zone, marked differences are found for corresponding non-zero F_c : in particular, for the excitations above 20 meV along the $Y-\Gamma$, $M-Y$ and $\Gamma-X$ paths. Furthermore, the magnon gap obtained with non-zero F_c is about 7 times larger than the one resulting if the correspondingly scaled A_d value (i.e. leading to equal classical energies) is used.

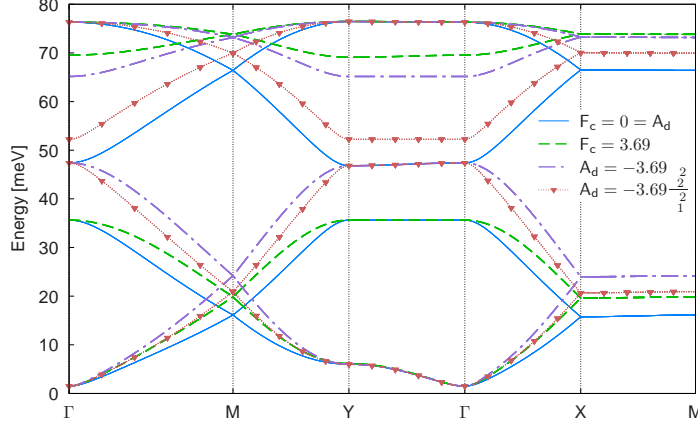


Figure 6. (color-online) Layered: Quantum intermediate phase magnons, for different A_d and F_c combinations (both considered FM). Other non-zero magnetic couplings, in meV: $F' (= F) = 9.98$, $A (= A') = 1.83$, $D = 0.05$, while spin magnitudes: $S_1 = 2$, and $S_2 = 1.5$ (as in Ref [21]). For: $F_c = 0$ and $A_d = 0$ (solid lines); $F_c = 3.69$ and $A_d = 0$ (dashed lines); $F_c = 0$ and $A_d = -3.69$ (dash-dotted lines); $F_c = 0$ and $A_d = -3.69 S_2^2/S_1^2$ (triangles). $\theta = 0$.

3.3.2. Bilayer compounds.

To fit their INS data in bilayer $\text{Pr}(\text{Ca}_{0.9}\text{Sr}_{0.1})_2\text{Mn}_2\text{O}_7$, Johnstone *et al.* [23] considered a localized spin model where they also included NNN couplings along the zig-zag chains: F_c and A_d in our notation of figure 1. Interestingly, they mentioned that one good fit can be achieved if no charge disproportionation is assumed ($S_1 = S_2$) and both A_d and F_c of almost identical magnitude are included: though with opposite signs, one of them AF and the other FM [23]. In this regard, they indicate that the excitation spectrum is unchanged by interchanging the values (and signs) of these two magnetic exchange parameters. In the Discussion section we will address these points in detail. Here, as a first step for that analysis, we illustrate the separate effects of these coupling parameters on the quantum intermediate phase magnons of bilayer compounds: in figure 7 we exhibit the effect of F_c , and in figure 8 we show the effect of A_d . Basically, we find that different magnon branches are affected by each of these two coupling parameters.

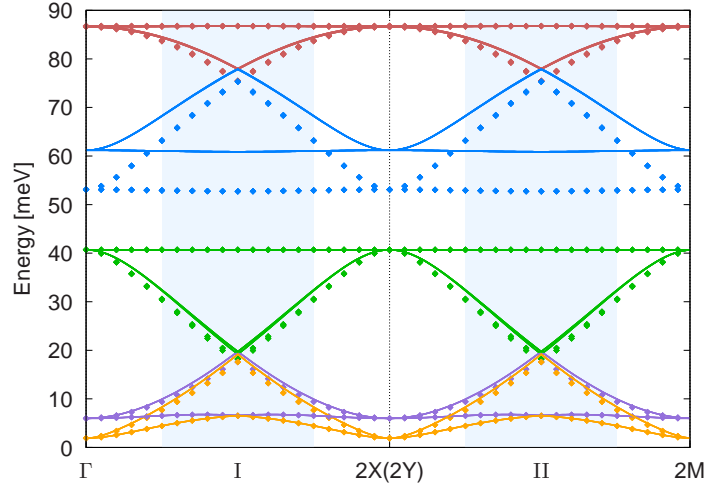


Figure 7. (color online). Bilayer: Effect of F_c on the quantum intermediate phase magnons. Non-zero magnetic couplings, in meV: $F' (=F) = 11.39$, $A (=A') = 1.5$, $A_z (=B_z) = 0.88$, $D = 0.074$; while: $F_c = 0$ (symbols), and $F_c = 1.35$ (solid lines). $S_1 = 2$, $S_2 = 1.5$. $\theta = 0$.

Concretely, figure 7 shows that increasing a ferromagnetic F_c mainly affects the magnon branches defining the top of the magnon gap (lifting it about 10 meV, in the case shown), while in the lower bands the effects are almost imperceptible. Furthermore, changing the sign of coupling F_c leads to the same magnon branches being affected, but the ensuing shift of energies has the opposite sign (and equal magnitude).

On the other hand, figure 8 illustrates that increasing an antiferromagnetic A_d coupling, mainly shifts the magnon branches defining the bottom of the magnon gap, reducing their energy (by about 12 meV, in the case shown), while all other magnon branches are almost unchanged. Again, changing the sign of coupling A_d leads to the same magnon branches being affected, but the ensuing shift of energies has opposite sign (and equal magnitude).

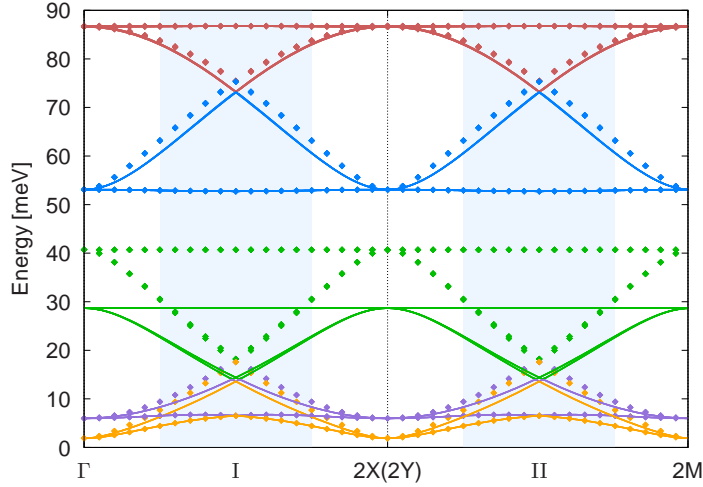


Figure 8. (color online). Bilayer: Effect of A_d on quantum intermediate phase magnons. Non-zero magnetic couplings, in meV: $F' (=F) = 11.39$, $A (=A') = 1.5$, $A_z (=B_z) = 0.88$, $D = 0.074$; while: $A_d = 0$ (symbols); and $A_d = 1.5$ (solid lines). $S_1 = 2$, $S_2 = 1.5$. $\theta = 0$.

Thus, our analysis demonstrates that the two coupling parameters F_c and A_d allow to fit the magnon gap, by tuning their magnitudes and signs. In particular, we have checked that in the absence of disproportionation, no magnon gap will exist if $F_c = 0 = A_d$. Furthermore, the separate effect of F_c and A_d on particular magnon branches up to now presented, allows to understand the statement of Johnstone *et al.* [23] regarding the possibility of interchanging their values and signs simultaneously for their fit. However, as we shall discuss in more detail in Section 4, we found that a complex interplay of these two couplings with the antiferromagnetic inter-chain coupling parameter A exists in the model, so that in a more general case, with larger values of A , one can not affirm that an interchange of F_c and A_d is always possible without affecting the magnon energies.

3.4. Effect of long-range inter-chain couplings: A_s and B_s

To end this section, we discuss the effect of the NNN coupling terms between the zig-zag chains which, to our knowledge, had not been included before in fits to INS results for half-doped manganites. In the following we will show our findings, in particular how each of them affects the different magnon branches. In section 4 we will discuss their relevance to obtain an improved fit for the magnetic excitations measured in $\text{Pr}(\text{Ca}_{0.9}\text{Sr}_{0.1})_2\text{Mn}_2\text{O}_7$.

Concretely, we decided to include these inter-chain NNN coupling parameters in the model, to be able to take into account spin differentiation (charge disproportionation) effects: A_s between S_2 - S_2 spins, and B_s between S_1 - S_1 spins.

As shown in figure 9, the main effect of non-zero antiferromagnetic A_s couplings between S_2 spins is to increase almost rigidly the energies of all upper magnon branches (those above the magnon gap), while the only most relevant change to energies of lower magnon branches (those below the magnon gap) is produced around BZ points I and II (lifting the lowest-energy magnon branch about 2 meV, at I and II).

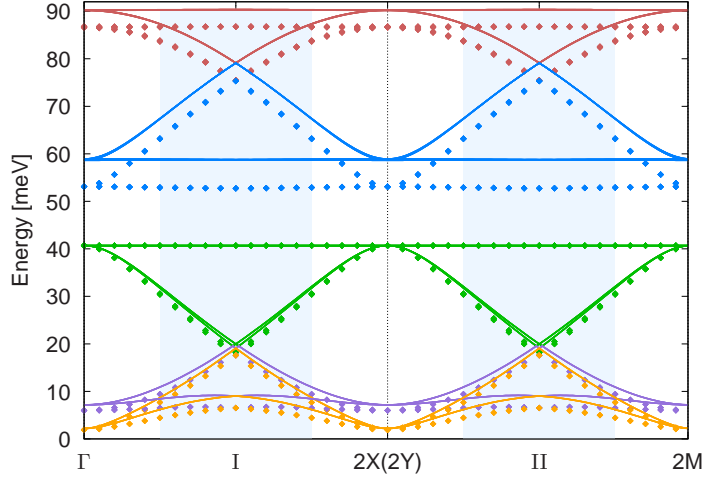


Figure 9. (color online). Bilayer: Effect of A_s on the quantum intermediate phase magnons. Non-zero magnetic couplings, in meV: $F'(=F)=11.39$, $A(=A')=1.5$, $A_z(=B_z)=0.88$, $D=0.074$; while: $A_s=0$ (symbols), and $A_s=2.0$ (solid lines). $S_1=2$, $S_2=1.5$. $\theta=0$.

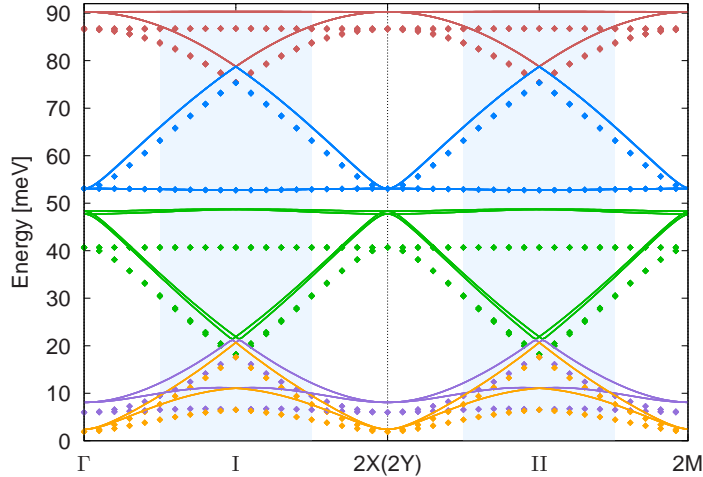


Figure 10. (color online). Bilayer: Effect of B_s on the quantum intermediate phase magnons. Non-zero magnetic couplings, in meV: $F'(=F)=11.39$, $A(=A')=1.5$, $A_z(=B_z)=0.88$, $D=0.074$; while: $B_s=0$ (symbols), and $B_s=2.0$ (solid lines). $S_1=2$, $S_2=1.5$. $\theta=0$.

As shown in figure 10 (for antiferromagnetic $B_s > 0$), the effect of B_s coupling between antiparallel S_1 - S_1 spins is more complex (than that of A_s), starting by the q -dependent shifts in the magnon branches. For instance, the lowest magnon branch, has a maximum increase in energy at BZ points I and II, while the magnons at Γ , $2X$, $2M$ are unaffected. The largest magnon change resulting from $B_s > 0$ is observed at the flat band corresponding to the bottom of the magnon gap, which is lifted rigidly by about 8 meV in figure 10. Changing the sign of this coupling: to ferromagnetic $B_s < 0$, results in a reversion of the effects on the magnons: the ensuing q -dependent shift of

energies has opposite sign (and equal magnitude). Notice that the magnon branch at 60 meV is unaffected along the whole BZ by the appearance of a non-zero B_s coupling.

4. Discussion

In this section, we will show some results which allow us to discuss and contribute to clarify a few important points relative to the nature of the ground state of half-doped manganites, still unresolved, which we could address using the model we considered.

i) First, we would like to return to the INS magnon measurements for layered $\text{La}_{0.5}\text{Sr}_{1.5}\text{MnO}_4$ by Senff *et al.* [21], and the comparison of fits to those data with different assumptions for the ground state. It is important to stress that only measurements for the lower magnon bands, below the magnon gap, were reported [21], based on which it was indicated [21] that a fully satisfactory fit was attained assuming that the ground state was Goodenough's CE phase of table 1 (with parameters: $F'(=F) = 9.98$, $A(=A') = 1.83$) complemented by the addition of a ferromagnetic coupling $F_c = 3.69$ between NNN intra-chain Mn^{4+} - Mn^{4+} pairs. We will denote this phase as CE-1, in the following, and in figure 11 have plotted as solid lines the magnons (lower and also upper bands) corresponding to this phase, while the black dots reproduce the experimental data by Senff *et al.* [21]. Next, we address the possibility, mentioned by Senff *et al.* [21], of obtaining an equally good fit for those experimental data in terms of a ground state which we will denote CE-2: consisting of Goodenough's CE phase of table 1 complemented by the addition of a ferromagnetic coupling A_d , between NNN intra-chain Mn^{3+} - Mn^{3+} pairs. In section 3.3 we analyzed and compared the separate effects of F_c and A_d . and showed that these two coupling parameters produced different quantum phase magnons, even if one chose them so as to preserve the scaling relation leading to equal classical results using one or the other (see figures 5 and 6). Thus, to achieve our best fit to the experimental INS data of Senff *et al.* [21] in terms of a CE-2 phase, which we included in figure 11 using dot-dashed lines, different magnitudes for the coupling parameters were needed: $F'(=F) = 7.18$, $A(=A') = 1.9$, $A_d = -3.0$. Finally, in figure 11 we also included our best fit to the experimental INS data of Senff *et al.* [21] in terms of ZP-dimer phase [13], like indicated in table 1, in which case: $F' = 21.58$, $F = 8.48$, $A(=A') = 1.98$.

Figure 11 illustrates two points very clearly: (i) knowledge limited to the lower magnon bands (below the gap) of the layered half-doped manganites is insufficient to determine unambiguously if their ground state corresponds to a CE (be it CE-1, or CE-2) or a ZP-dimer phase. We show that it is possible to attain equally good fits to the magnon branches below the gap with these three proposed ground states (the fits mainly differ (and only slightly) along the $X - M$ path in the BZ: where there are no experimental data [21]); (ii) it is the pending measurement of the upper magnon bands (above the magnon gap) which would unambiguously allow to recognize if the nature of the ground state of the layered half-doped manganites is CE or ZP-dimer like. This conclusion is in agreement with what Johnstone *et al.* [23] found for half-doped bilayer compounds.

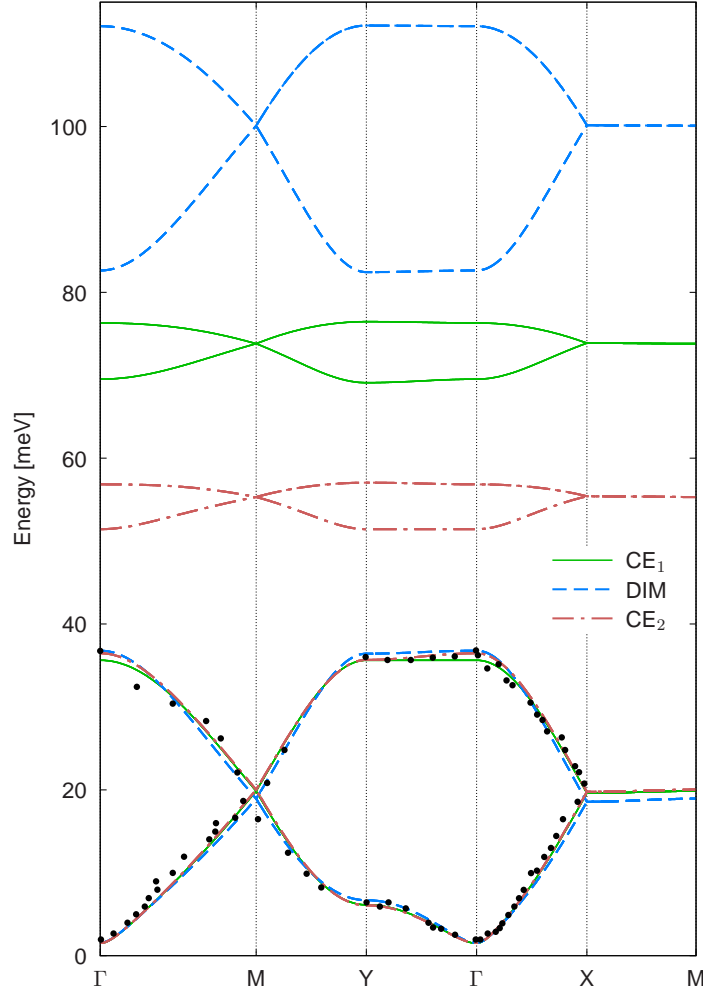


Figure 11. (color-online) Layered: Quantum magnons for $\text{La}_{0.5}\text{Sr}_{1.5}\text{MnO}_4$. Non-zero magnetic couplings in meV, and spin magnitudes, calculated for three proposed phases, respectively: CE_1 phase (solid lines): $F' (= F) = 9.98$, $A (= A') = 1.83$, $F_c = 3.69$, $S_1 = 2$, $S_2 = 1.5$, fit by Senff *et al.* [21]; ZP dimer - phase (dashed lines): $F' = 21.58$, $F = 8.48$, $A (= A') = 1.98$, $S_1 = S_2 = 1.75$; CE_2 phase (dash-dotted lines): $F' (= F) = 7.18$, $A (= A') = 1.9$, $A_d = -3.0$, $S_1 = 2$, $S_2 = 1.5$. $\theta = 0$. INS experimental points by Senff *et al.* [21] included (black dots).

ii) Next, for bilayer compounds, we will discuss in detail the joint effect of the NNN intra-chain couplings F_c and A_d , and under which conditions it is possible to interchange their magnitudes and signs, as mentioned by Johnstone *et al.* [23], without affecting the magnon spectrum. As mentioned in section 3.3 and seen in figure 12, the angle θ that minimizes the classical energy and K_c do not change when we interchange the values and signs of A_d and F_c , if the spin magnitudes are equal: $S_1 = S_2$, with parameters like Johnstone *et al.* [23] had mentioned. However, we have found that this statement must be revised in the quantum case in general, and especially when $S_1 \neq S_2$.

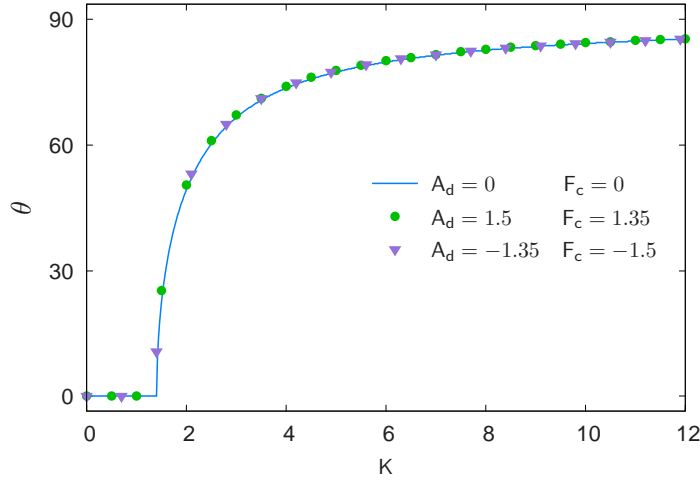


Figure 12. (color online). Bilayer: Angle characteristic of the classical intermediate phase with minimal energy, as a function of K : for $S_1 = S_2 = 1.75$, and different A_d and F_c combinations, as detailed in inset. Non-zero magnetic couplings, in meV: $F' = 11.39$, $A = 4.0$, $A_z (= B_z) = 0.88$, $D = 0.074$. F and A' as in equations (1a). For: $A_d = 0$, $F_c = 0$ (solid line); $A_d = 1.5$, $F_c = 1.35$ (dots); $A_d = -1.35$, $F_c = -1.5$ (triangles).

For instance, in figure 13 we compare the quantum magnons under the interchange of F_c and A_d , for two cases with equal classical results (see figure 12), and A larger than in the previous figures, in order to make the effect more visible. Here $S_1 = S_2$, and even though the magnon spectra are quite similar, there are differences in some regions of the BZ (see shaded region, e.g.), and also the non-dispersive modes (flat magnon bands) of each case are located in different bands. Specifically, when $F_c = 1.35$ and $A_d = 1.5$ meV the flat band lies at the bottom of the magnon gap (~ 45 meV), while when we interchange the values and signs of these couplings, it is now placed at the top of the gap (~ 65 meV). It is interesting to stress that the differences found, allow to determine the appropriate signs for A_d and F_c in our model which, according to the experimental data [23], would then correspond to an antiferromagnetic A_d and a ferromagnetic F_c .

The effects discussed above, become amplified if the spins are of different magnitudes, and again using a larger value of A , since this causes more dispersion in the bands near the top or the bottom of the gap. Figure 14 shows that with $S_1 \neq S_2$, classically, angle θ and also K_c are different under interchange of F_c and A_d . Not surprisingly, the corresponding quantum excitation spectra, which we show in figure 15, differ even more between them: e.g. the shift observed in the flat band modes has been noticeably increased.

iii) For bilayer $\text{Pr}(\text{Ca}_{0.9}\text{Sr}_{0.1})_2\text{Mn}_2\text{O}_7$ [23], we will now present two other possible fits for the INS measurements by Johnstone[23], the last one representing the best fit to the experimental results yet, to our knowledge.

First, in figure 16 we present a fit to the magnons measured in $\text{Pr}(\text{Ca}_{0.9}\text{Sr}_{0.1})_2\text{Mn}_2\text{O}_7$ [23] which we obtained using our model with $K \neq 0$ and $\theta = 0$. Except for the inclusion of K , the coupling magnitudes here used are quite similar to those used by Johnstone *et al.* [23], i.e. the ratios between the couplings are similar, and our fit to the experimental data shown in figure 16 is almost indistinguishable

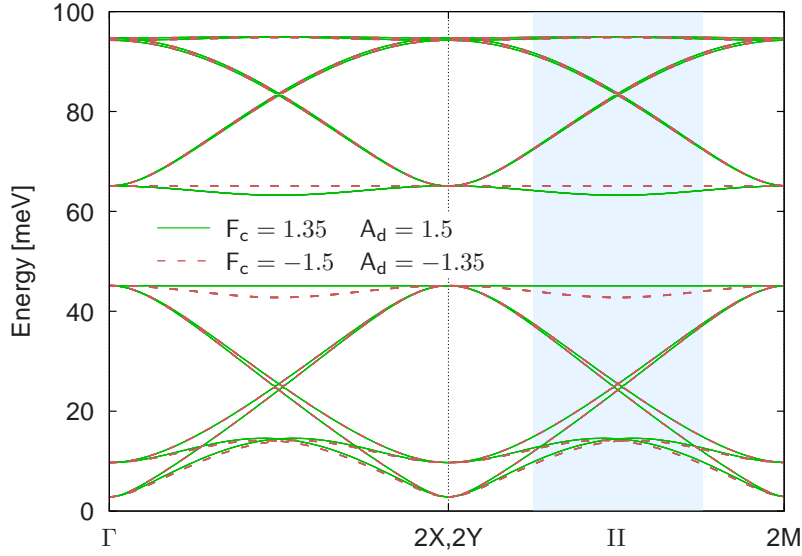


Figure 13. (color online) Bilayer: Magnons calculated for different combinations of A_d and F_c , with: $S_1 = S_2 = 1.75$. Nonzero magnetic couplings, in meV: $F' (= F) = 11.39$, $A (= A') = 4.0$, $D = 0.074$, $A_z = B_z = 0.88$; for: $F_c = 1.35$, $A_d = 1.5$ (solid lines); $F_c = -1.5$, $A_d = -1.35$ (dashed lines). $\theta = 0$.

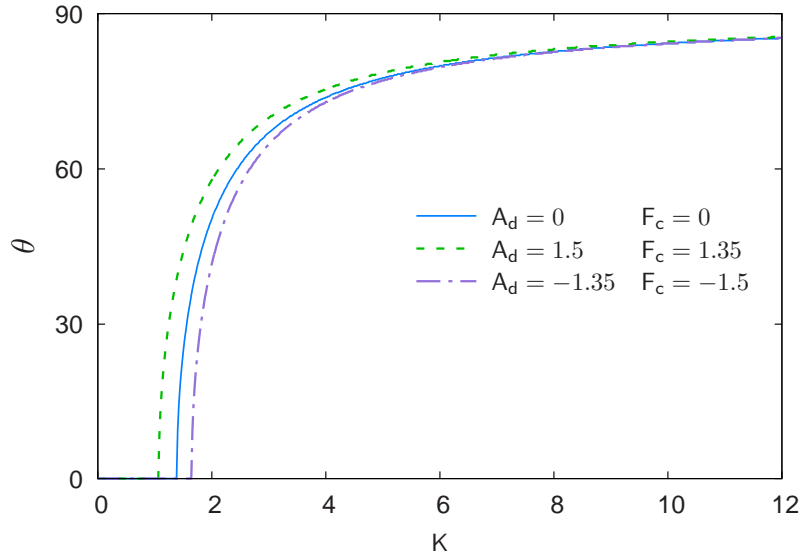


Figure 14. (color online). Bilayer: Angular dependence of the energy of the classical intermediate phase, for different A_d and F_c combinations. Non-zero magnetic couplings, in meV: $F' = 11.39$, $A = 4.0$, $A_z (= B_z) = 0.88$, $D = 0.074$, $A_z (= B_z) = 0.88$, F and A_p as in equations (1a) and S_1, S_2 as in equations (1b). $A_d = 0$, $F_c = 0$ (solid line), $A_d = 1.5$, $F_c = 1.35$ (dashed-line); $A_d = -1.35$, $F_c = -1.5$ (dash-dotted line).

from their own fit. Nevertheless, the present fit has the advantage that it involves a charge disproportionation ($\delta = 0.5$: thus Mn^{3+} and Mn^{4+} would be present) within

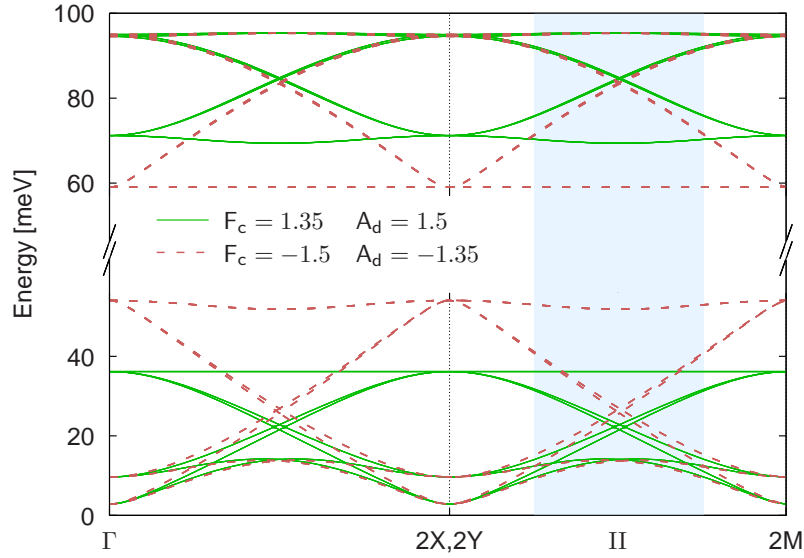


Figure 15. (color online) Bilayer: Magnons calculated for different combinations of A_d and F_c , with $S_1 = 2$ and $S_2 = 1.5$. Non-zero magnetic couplings, in meV: $F' (= F) = 11.39$, $A (= A') = 4.0$, $D = 0.074$, $A_z = B_z = 0.88$. For: $F_c = 1.35$, $A_d = 1.5$ (solid lines); $F_c = -1.5$, $A_d = -1.35$ (dashed lines). $\theta = 0$.

the range proposed by Goodenough [8] and most other experiments [15, 25], even without including NNN couplings like A_d or F_c : as proposed by Senff *et al.* [21], Ulbrich *et al.* [22] and Johnstone *et al.* [23] for their best fits. We use $\theta=0$, which is the angle corresponding to the minimum of the classical energy for the intermediate phase, with these parameters.

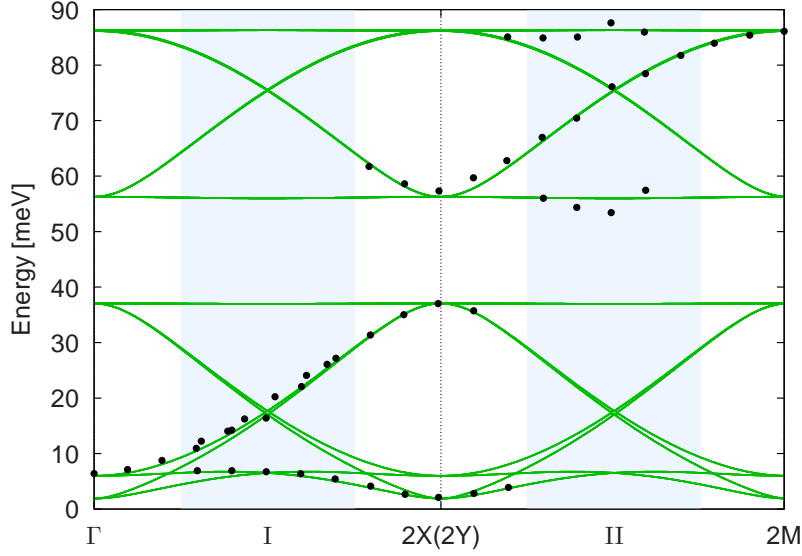


Figure 16. (color online) Bilayer: best fit to the experimental magnon data [23] (included as black dots) in terms of an intermediate phase with non-zero biquadratic coupling K , describing the data like the fit by Johnstone *et al.* [23]. Non-zero couplings, in meV: $F' (= F) = 13.45$, $A (= A') = 1.5$, $A_z (= B_z) = 0.88$, $K = 1.7$, $D = 0.08$. Spin magnitudes: $S_1 = 2$ and $S_2 = 1.5$ (i.e. $\delta = 0.5$). $\theta = 0$.

Finally, we present the best fit which we obtained for the INS data for magnons in the half-doped bilayer manganite $\text{Pr}(\text{Ca}_{0.9}\text{Sr}_{0.1})_2\text{Mn}_2\text{O}_7$ [23] after our thorough exploration of parameter ranges and different phases for the localized spin model here studied. In figure 17 we exhibit the calculated magnons, comparing them with the experimental data by Johnstone *et al.* [23]. An improvement with respect to previous fits, is given by the fact that we are also able to describe the dispersion in the shaded region near II which is clearly present in the measured upper magnon bands (above the gap): we find this is due to our inclusion of NNN inter-chain couplings A_s and B_s , and their delicate interplay with the value of NN inter-chain coupling A for the determination of the gaps and dispersion of the bands near I and II. Our best fit to the experimental data in half-doped bilayer compounds [23] appears represented by figure 17, and corresponds to a generalized CE phase, with the following non-zero magnetic couplings (in meV): $F' (= F) = 10.89$, $A (= A') = 3.6$, $A_z (= B_z) = 0.88$, $A_s = 0.5$, $B_s = -3.4$ and $D = 0.074$. For this particular phase, we did not use equations (1b) for the spin magnitudes, instead we found that we optimized our fit with: $S_1 = 1.8$ and $S_2 = 1.7$ (i.e. $\delta = 0.2$), and $\theta = 0$.

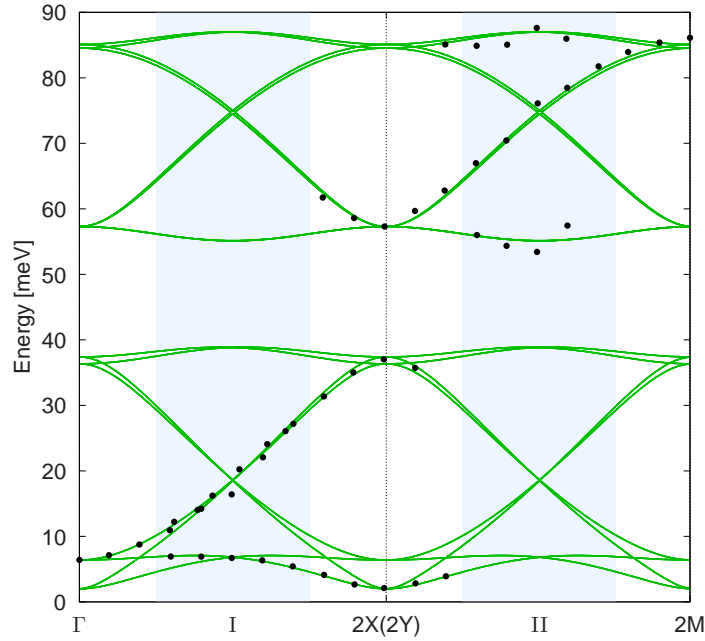


Figure 17. (color online) Bilayer: our best fit to the INS data for magnons[23] (included as dots), using a generalized CE phase: including NNN couplings between zig-zag chains but not along the chains. Non-zero magnetic couplings, in meV: $F'(=F) = 10.89$, $A(=A') = 3.6$, $A_z(=B_z) = 0.88$, $A_s = 0.5$, $B_s = -3.4$, $D = 0.074$. For this phase, we did not use equations (1b) for the spin magnitudes, instead: $S_1 = 1.8$ and $S_2 = 1.7$ (i.e. $\delta = 0.2$). $\theta = 0$.

5. Conclusions

We have studied the spin excitations of a model of interacting localized spins for the description of the intermediate phase of half-doped bilayer manganites such as $\text{Pr}(\text{Ca}_{0.9}\text{Sr}_{0.1})_2\text{Mn}_2\text{O}_7$, for which experimental inelastic neutron scattering data were recently obtained [23], and have compared our results also with the data reported for layered half-doped manganites such as $\text{La}_{0.5}\text{Sr}_{1.5}\text{MnO}_4$ [21]. The model investigated includes magnetic couplings between Mn-ions up to second neighbors in the zig-zag chains as well as between zig-zag chains, allowing us to compare in detail the main effect of the different couplings on the magnons, including in particular all coupling parameters previously used to fit experimental INS data in half-doped manganites by other groups. The model we proposed for the intermediate phase introduced by Efremov et al [26] allows to discuss different degrees of Mn-charge disproportionation, as well as relative orientation of consecutive spin dimers along a zig-zag chain, describing Goodenough's original [8] (and also generalized) CE phases, theoretically also the orthogonal intermediate- $\pi/2$ dimer phase [26], and the Zener-polaron dimer phase [13]. We had studied a simpler version of the model previously [30], for layered half-doped manganites such as $\text{La}_{0.5}\text{Sr}_{1.5}\text{MnO}_4$.

For classical spins, we find that an intermediate phase characterized by non-zero angle θ is stable only for biquadratic inter-dimer couplings above a critical value K_c , which decreases with increasing coupling between the zig-zag chains (A and A'). For quantum spins, the stability of the intermediate phase is reduced to a more limited

range of angles, being K the most relevant parameter for stability. In particular, we could not find any set of parameters for which the quantum $\theta = \pi/2$ orthogonal dimer phase [26] was stable.

Calculating the quantum magnons of the intermediate phase, we could also analyze those corresponding to Goodenough's original and generalized CE phases, and we also studied the Zener-polaron dimer phase, discussing our results in the context of recent experimental results for layered and bilayer half-doped manganites. In particular, for the layered compounds, we show that important differences would appear in the yet unmeasured magnon bands above the gap for CE phases and the Zener-polaron dimer phase, which would allow to unambiguously distinguish between them, while the measured lower magnon bands can almost be equally well described by any of these phases. Therefore, we consider that, at least on the basis of the available magnon data for layered half-doped manganites, one can not exclude any of the proposals for the ground state, in particular a ZP-dimer phase, while experimental magnon data where the differences would be easily distinguishable are not yet available at higher energies. Based on our estimations of figure 11, this would require INS measurements in layered half-doped manganites in the range of energies above 40 meV, similar to the range where the bilayer upper magnon bands were measured [23].

We have presented an improved description of the magnons reported for half-doped bilayer manganites [23], in terms of a generalized CE phase ($\theta = 0$) having Mn-disproportionation within the expected range ($\delta = 0.2 \leq 0.5$), in agreement with most of the experimental evidence and in contrast to Johnstone *et al.* [23] which in their fit had: $\delta = 0.82$ (i.e.: $\text{Mn}^{2.68+}$ and $\text{Mn}^{4.32+}$). We also found that the introduction of next-nearest-neighbour magnetic coupling between the planar Mn zig-zag chains and an appropriate tuning of the nearest-neighbour inter-chain antiferromagnetic coupling, are the relevant factors needed to reproduce the additional dispersion exhibited by the measured magnons, which had not been described previously [23].

6. Acknowledgements

We acknowledge financial support by CONICET (PIP grant 0702, and a fellowship awarded to I.R.B.). L.O.M. and C.I.V. are members of Carrera del Investigador Científico, CONICET.

References

- [1] R. Kajimoto, H. Yoshizawa, H. Kawano, H. Kuwahara, Y. Tokura, K. Ohoyama, and M. Ohashi. *Phys. Rev. B*, 60:9506–9517, (1999).
- [2] E. Dagotto, T. Hotta, and A. Moreo. *Phys. Rep.*, 344:1–153, (2001).
- [3] J. Hemberger, A. Krimmel, T. Kurz, H-A. Krug von Nidda, V. Y. Ivanov, A. A. Mukhin, A. M. Balbashov, and A. Loidl. *Phys. Rev. B*, 66:094410, 2002.
- [4] S. Larochelle, A. Mehta, L. Lu, P. K. Mang, O. P. Vajk, N. Kaneko, J. W. Lynn, L. Zhou, and M. Greven. *Phys. Rev. B*, 71:024435, (2005).
- [5] Y. Tokura. *Rep. Prog. Phys.*, 69:797, (2006).
- [6] Y. Moritomo, A. Asamitsu, H. Kuwahara, and Y. Tokura. *Nature*, 380:141–144, (1996).
- [7] S. Kawano, N. Achiwa, N. Kamegashira, and M. Aoki. *J. Phys. Colloques*, 49:C8–829–C8–830, (1988).
- [8] J. B. Goodenough. *Phys. Rev.*, 100:564, (1955).
- [9] C. Zener. *Phys. Rev.*, 82:403–405, (1951).
- [10] P. G. Radaelli, D. E. Cox, M. Marezio, and S-W. Cheong. *Phys. Rev. B*, 55:3015–3023, (1997).
- [11] Y. Murakami, H. Kawada, H. Kawata, M. Tanaka, T. Arima, Y. Moritomo, and Y. Tokura. *Phys. Rev. Lett.*, 80:1932–1935, (1998).

- [12] S. Di Matteo, T. Chatterji, Y. Joly, A. Stunault, J. A. Paixao, R. Suryanarayanan, G. Dhahlenne, and A. Revcolevschi. *Phys. Rev. B*, 68:024414, (2003).
- [13] A. Daoud-Aladine, J. Rodríguez-Carvajal, L. Pinsard-Gaudart, M. T. Fernández-Díaz, and A. Revcolevschi. *Phys. Rev. Lett.*, 89:097205, (2002).
- [14] S. Grenier, J. P. Hill, D. Gibbs, K. J. Thomas, M. V. Zimmermann, C. S. Nelson, V. Kiryukhin, Y. Tokura, Y. Tomioka, D. Casa, T. Gog, and C. Venkataraman. *Phys. Rev. B*, 69:134419, (2004).
- [15] K. J. Thomas, J. P. Hill, S. Grenier, Y.-J. Kim, P. Abbamonte, L. Venema, A. Rusydi, Y. Tomioka, Y. Tokura, D. F. McMorrow, G. Sawatzky, and M. van Veenendaal. *Phys. Rev. Lett.*, 92:237204, (2004).
- [16] E. L. Winkler, M. Tovar, and M. T. Causa. *J. Phys. Condens. Matter*, 25(29):296003, (2013).
- [17] J. Herrero-Martín, J. García, G. Subías, J. Blasco, and M. C. Sánchez. *Phys. Rev. B*, 70:024408, (2004).
- [18] G. Subías, J. García, P. Beran, M. Nevřiva, M. C. Sánchez, and J. L. García-Muñoz. *Phys. Rev. B*, 73:205107, (2006).
- [19] J. Herrero-Martín, J. García, J. Blasco, and G. Subías. *Eur. Phys. J. Special Topics*, 208:107–119, (2012).
- [20] C. I. Ventura and B. Alascio. *Phys. Rev. B*, 68:020404, (2003).
- [21] D. Senff, F. Krüger, S. Scheidl, M. Benomar, Y. Sidis, F. Demmel, and M. Braden. *Phys. Rev. Lett.*, 96:257201, (2006).
- [22] H. Ulbrich, F. Krüger, A. A. Nugroho, D. Lamago, Y. Sidis, and M. Braden. *Phys. Rev. B*, 84:094453, (2011).
- [23] G. E. Johnstone, T. G. Perring, O. Sikora, D. Prabhakaran, and A. T. Boothroyd. *Phys. Rev. Lett.*, 109:237202, (2012).
- [24] C. Jardón, F. Rivadulla, L. E. Hueso, A. Fondado, M. A. López-Quintela, J. Rivas, R. Zysler, M. T. Causa, and R. D. Sánchez. *J. Magn. Magn. Mater.*, 196–197:475–476, (1999).
- [25] S. Mercone, A. Wahl, A. Pautrat, M. Pollet, and C. Simon. *Phys. Rev. B*, 69:174433, (2004).
- [26] D. V. Efremov, J. van den Brink, and D. I. Khomskii. *Nat Mater*, 3:853–856, (2004).
- [27] G. Giovannetti, S. Kumar, J. van den Brink, and S. Picozzi. *Phys. Rev. Lett.*, 103:037601, (2009).
- [28] P. Barone, S. Picozzi, and J. van den Brink. *Phys. Rev. B*, 83:233103, (2011).
- [29] K. Yamauchi and S. Picozzi. *J. Phys. Soc. Jpn.*, 82:113703, (2013).
- [30] I. R. Buitrago, C. I. Ventura, and L. O. Manuel. *IEEE Trans. Magn.*, 49:4691–4694, (2013).
- [31] I. R. Buitrago and C. I. Ventura. *J. Supercond. Nov. Magn.*, 26:2303–2305, (2013).
- [32] J. H. P. Colpa. *Physica A: Statistical Mechanics and its Applications*, 93:327–353, (1978).
- [33] M. Cieplak. *Phys. Rev. B*, 18:3470–3485, (1978).
- [34] A. L. Wysocki, K. D. Belashchenko, and V. P. Antropov. *Nat Phys*, 7:485–489, (2011).
- [35] D. Stanek, O. P. Sushkov, and G. S. Uhrig. *Phys. Rev. B*, 84:064505, (2011).
- [36] J. Chaloupka and G. Khaliullin. *Phys. Rev. Lett.*, 110:207205, (2013).
- [37] S. O. Diallo, V. P. Antropov, T. G. Perring, C. Broholm, J. J. Pulikkotil, N. Ni, S. L. Bud'ko, P. C. Canfield, A. Kreyssig, A. I. Goldman, and R. J. McQueeney. *Phys. Rev. Lett.*, 102:187206, (2009).
- [38] J. Zhao, D. T. Adroja, D. Yao, R. Bewley, S. Li, X. F. Wang, G. Wu, X. H. Chen, J. Hu, and P. Dai. *Nat Phys*, 5:555–560, (2009).